

## A technique for rapid calibration of crossed-hot-wires

S. M. Henbest<sup>1</sup>, M. B. Jones<sup>1</sup> and J. H. Watmuff<sup>2</sup>

<sup>1</sup>Aerospace Division, Defence Science & Technology Group  
Victoria 3207, Australia

<sup>2</sup>School of Engineering  
RMIT University, Victoria 3083, Australia

### Abstract

A method for the calibration of a crossed-hot-wire probe is presented. The method involves a full calibration of around 25 data points, from which the effective wire angles and longitudinal cooling coefficients are determined. These values are used in calculating the effective cooling velocities. As long as the effective wire angles and longitudinal cooling coefficients are invariant, then subsequent calibrations only require measurement of effective cooling velocity against anemometer output voltages and accurate X-wire calibrations can be obtained using as few as 7 data points.

### Introduction

Hot-wire anemometry is a method used to infer fluid velocity [11], [10], [2] from the output voltage of an anemometer circuit that heats a micron-sized sensing element, known as a hot-wire.

A X-wire probe consists of two hot-wires laying in closely spaced parallel planes such that they form an 'X' with a nominal included angle of  $90^\circ$  as shown in Figure 1. The X-wire allows both the direction and magnitude of the instantaneous velocity to be resolved in the plane of the wires; however, any out of plane velocity can lead to bi-normal cooling and errors in the inferred in-plane velocities [15].

There are several different approaches to calibrating X-wires ([3], [1]) which can be classed as either: (i) physically based mathematical model, (ii) polynomial based mathematical model or (iii) interpolation. The degrees-of-freedom in these models (unknown parameters) increases from class (i) through to class (iii) which necessitates a corresponding increase in the number of calibration points required.

The calibration of crossed-hot-wires can be a time consuming process, especially for highly turbulent flow experiments where a wide range of flow velocity vectors are anticipated. Additionally, in experiments where flow temperature changes, pre- and post-calibrations are required. Here a method for the rapid calibration of crossed hot-wires is presented.

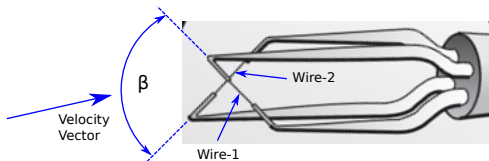


Figure 1: X-wire probe where the wires lay in planes parallel to the page and form an included angle  $\beta$  (illustration adapted from [9]).

### Calibration Method

In this paper we propose a calibration method which combines aspects of classes (i) and (ii) and we identify the model parameters that are invariant (and depend upon physical factors such

as probe geometry) from those parameters that may either drift with temperature or time. A full calibration is performed where all parameters are determined and thereafter a subset calibration where only the non-invariant parameters are determined.

Figure 2 shows a hot-wire inclined at angle  $\psi$  to the probe axis. The wire is exposed to a velocity vector with components  $U$  and  $V$  in the  $x$  and  $y$  directions respectively. The effective cooling velocity is dominated by the velocity component normal to the wire. However, it has been shown by [5] that the velocity component longitudinal to the wire also has an influence on the cooling and hence the effective cooling velocity,  $U_e$ , is given by

$$U_e = \sqrt{(U \cos \psi + V \sin \psi)^2 + k^2(-U \sin \psi + V \cos \psi)^2}, \quad (1)$$

where  $k$  is a constant that accounts for the longitudinal cooling effect and has been found to depend on the length to diameter ratio of the wire and the velocity [5, 8, 14].

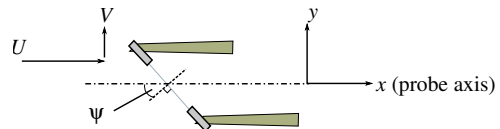


Figure 2: Inclined hot-wire at angle  $\psi$  to the probe axis.

The value of  $\psi$  is often taken to be the geometric angle of the wire to the probe axis. However, [13] proposed the cosine cooling law can be compensated for by using an effective wire angle,  $\psi_e$ , determined by tilting the probe and setting  $k = 0$  in (1). The benefits are that the calibration inversion is greatly simplified because the measurements are linearly dependent on the cooling velocity of each wire and once  $\psi_e$  are determined a static calibration can be used. This approach was shown to reduce the measurement error to acceptably small values as long as the turbulence intensities were moderate,  $u'/U < 20\%$ .

The method proposed here and described below has the same advantages, however, it fully accounts for the longitudinal cooling effect. The method is shown to significantly increase the measurement flow cone angle [12] and thus can be applied in more highly turbulent flows.

### Full calibration

The full calibration involves pitching the hot-wire probe at angles,  $\theta$ , across freestream velocities,  $U_\infty$ , which generates velocity components in the probe body-axis given by

$$U = U_\infty \cos(\theta), \quad V = -U_\infty \sin(\theta), \quad (2)$$

where  $\theta$  positive is defined as a pitch down. Substituting (2) into (1) leads to an effective cooling velocity of

$$U_e = U_\infty \left[ (\cos^2(\psi_e + \theta) + k^2 \sin^2(\psi_e + \theta)) \right]^{1/2}. \quad (3)$$

A cubic function, of the form

$$U_e = a_0 + a_1 E + a_2 E^2 + a_3 E^3, \quad (4)$$

is used to model the relationship between the effective cooling velocity and the anemometer output voltage,  $E$ , where  $a_0, \dots, a_3$  are fit parameters to be determined. Substituting (4) into (3) gives

$$U_\infty = \frac{a_0 + a_1 E + a_2 E^2 + a_3 E^3}{\sqrt{\cos^2(\psi_e + \theta) + k^2 \sin^2(\psi_e + \theta)}}. \quad (5)$$

A non-linear least-squares surface fit,  $U_\infty = U_\infty(E, \theta)$ , is used to determine the six fit parameters:  $\psi_e, k, a_0, \dots, a_3$ , for each wire.

The optimisation relies on choosing calibration points  $(\theta, U_\infty)$  such that the anticipated  $U_e$  values for different probe pitch settings have some degree of overlap. Further the anemometer voltage output domain of the calibration points should span the domain of voltages anticipated during the experiment. It is found around  $N = 25$  calibration points is sufficient to achieve a well defined minimum in the optimisation algorithm that determines the six fit parameters.

#### Subset calibration

During a subset calibration only the cubic coefficients in (4) are determined and  $\psi_e, k$  for each wire are held fixed at the values determined from the full calibration. The subset calibration is used to correct for temperature changes and small changes in wires properties which effect only the cubic coefficients.

To determine the coefficients accurately requires that the anemometer calibration voltages span the domain anticipated during the experiment. Depending on the calibration facility these voltages may be achieved by either holding the wires at fixed  $\theta = 0$  position and running the facility at sufficiently low and high velocities,  $U_\infty$ , or by varying both  $U_\infty$  and  $\theta$ .

At a minimum,  $N = 4$  calibration points are required for the cubic regression. However, it is suggested that  $N = 6$  to 10 be used for a more accurate calibration.

### Calibration Examples

#### Full Calibration Example

Figure 3 shows the anemometer output voltages  $E_2$  versus  $E_1$ , for a  $N = 24$  point calibration. Let us consider various data

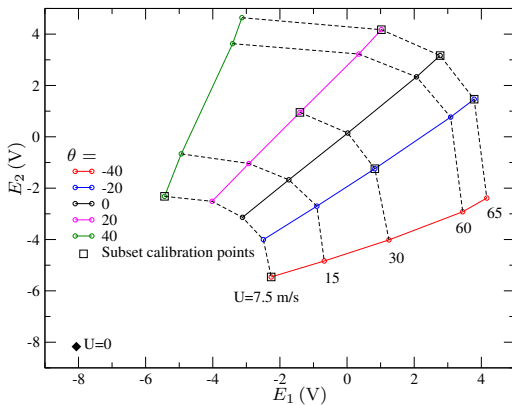


Figure 3: Anemometer output voltages during calibration.

calibration options based upon (3) and (4) using the data in Figure 3. Consider the method i.e. where  $k = 0$  applied to wire 1 data, a best-fit between  $U_e$  and  $E_1$  is obtained for a value of

$\psi_{e1} = 46.5^\circ$ , as shown in Figure 4(a). The collapse to (4) is only fair at higher values of  $U_e$ , most probably owing to the inclusion of calibration data at pitch angles close to the wire angle where the assumption of no longitudinal cooling breaks down. It has been pointed out [13] that the cosine cooling law assumption should only be used when the flow angle remains well within the included angle of the X-wires. Therefore, it would be reasonable to exclude this data when determining  $\psi_{e1}$ , and the calibration constants. The result is shown in Figure 4(b), the collapse is considerably better and a value of  $\psi_{e1} = -49.0^\circ$  is returned.

Including longitudinal cooling requires estimates of the cooling factor  $k$  and wire angles  $\psi_{e1}$  and  $\psi_{e2}$ . Here initial values of  $k = 0.2$  and the nominal physical wire angles of  $\psi_{e1} = 45^\circ$  and  $\psi_{e2} = -45^\circ$  were assumed. The estimated  $U_e$  values for wire-1, calculated using (3), are shown in Figure 5(a) and they form a series of overlapping curves which fail to collapse, indicating the estimated values for  $k$  and  $\psi_{e1}$  are sub-optimal.

Applying an iterative non-linear least-squares fitting routine [7], to the model function (5), gave best estimates of  $k_1 = 0.05$ ,  $\psi_{e1} = 49.3^\circ$  along with best estimates for the cubic coefficients  $a_0, \dots, a_3$ . Based on the optimised values ( $k_1, \psi_{e1}$ ), the effective cooling velocity acting on wire-1 is plotted in Figure 5(b) and good collapse is achieved. Applying the same process to wire-2 returned values of  $k_2 = 0.06$ ,  $\psi_{e2} = -45.9^\circ$  along with values for  $a_0, \dots, a_3$ .

To test the pitch angle limits of the X-wire (and also when anemometer voltage rectification occurs) the cross wire probe was pitched from  $\theta = -48^\circ$  to  $48^\circ$ , in a constant free stream velocity of 45 m/s and Figure 6 shows how the anemometer voltages varied. Local minimums occur at angles  $\theta = 43.6^\circ$  and  $= -45.5^\circ$  for wires 1 and 2, respectively. These angles define the cone angle and are on average approximately  $2.1^\circ$  degrees greater in magnitude than than the angles predicted using the effective wire angles (i.e.  $\pi/2 - \psi_{e1}$ ,  $-\pi/2 - \psi_{e2}$ ).

Using (4) and (3) together with the cooling and calibration constants for wire 1 and wire 2 determined above, the output voltages  $E_1$  and  $E_2$  can be predicted and these are also shown in Figure 6. For wire 1 the data agrees well up angles of up to  $30^\circ$  and for wire 2 up to angles of  $-40^\circ$ , at even higher angles the errors are not large. Also shown are the predicted voltages using  $k = 0$  and values of  $\psi_{e1}$  and  $\psi_{e2}$  determined as shown in Figure 4(b).

#### Subset Calibration Example

A subset of 7 calibration points was selected from the original 24 points. The subset is indicated by the square symbols of Figure 3.

The effective cooling velocities for the subset data were calculated using (3), using the values of  $k$  and  $\psi_e$  established during the full calibration and as given above. The cubic equation (4) was then fitted to the  $(U_e, E)$  data and new set of cubic coefficients. The difference between the cubic coefficients determined in the full and subset calibrations was negligible.

### Solution of Calibration Functions

Given an instantaneous measurement of anemometer voltages  $(E_1, E_2)$ , the effective velocities for each wire can be calculated using (4), where each wire has a unique set of cubic coefficients  $a_0, \dots, a_3$  associated with it. It is convenient to use the velocity magnitude,  $U_m = \sqrt{U^2 + V^2}$ , and velocity direction,  $\theta$  as the unknown variables since it allows an analytic solution to be obtained. In terms of these variables, the simultaneous equations

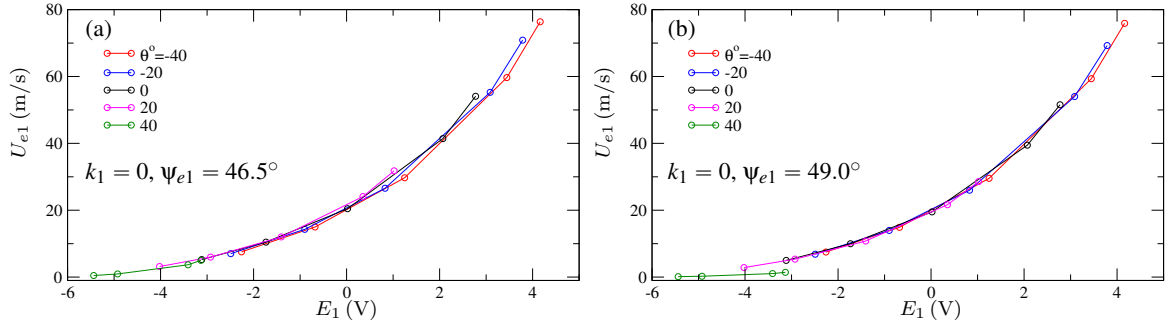


Figure 4:  $E_1$  versus  $U_e$  based on cosine cooling law: (a)  $k = 0$  and (b)  $k = 0$  and neglecting  $\theta = 40^\circ$  data

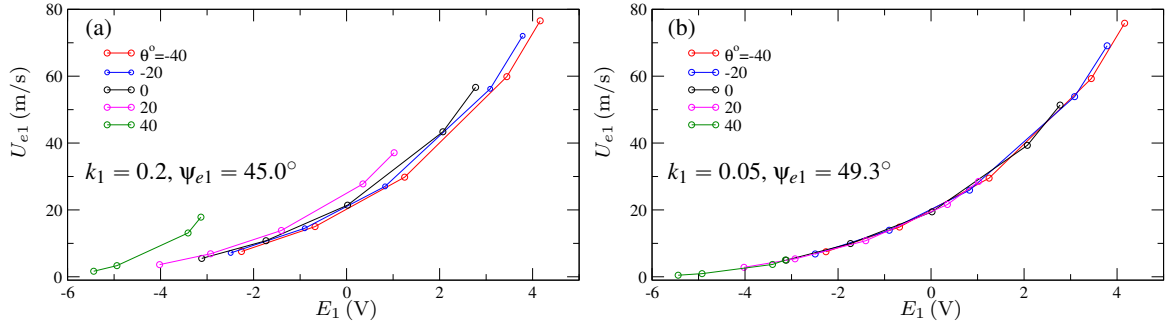


Figure 5:  $E_1$  versus  $U_e$  for: (a)  $k = 0.2$  and  $\psi_{e1} = 45^\circ$  (b) optimised  $k$  and  $\psi_{e1}$  values.

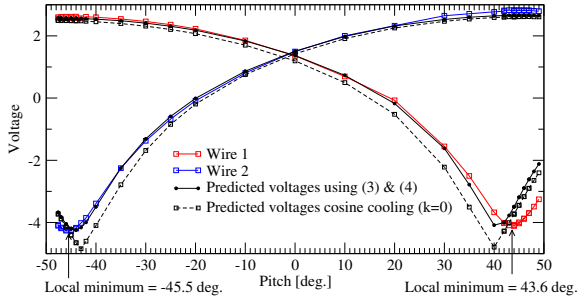


Figure 6: Anemometer voltages as probe is pitched in a constant velocity freestream flow. Local minima of the experimental data are shown.

to solve are then given by

$$U_{e1} = U_m \sqrt{\cos^2(\psi_{e1} + \theta) + k_1^2 \sin^2(\psi_{e1} + \theta)} \quad (6)$$

$$U_{e2} = U_m \sqrt{\cos^2(\psi_{e2} + \theta) + k_1^2 \sin^2(\psi_{e2} + \theta)}, \quad (7)$$

where subscript 1 and 2 denote wire-1 and wire-2, respectively. Eliminating  $U_m$  by dividing (6) by (7) gives a function of the form

$$(U_{e1}/U_{e2})^2 = f(\theta, k_1, k_2, \psi_{e1}, \psi_{e2}) \quad (8)$$

and this function is plotted in Figure 7 for wire parameters  $\psi_{e1} = -\psi_{e2} = 45^\circ$  and  $k_1 = k_2 = 0.1$ . Depending on the ratio  $(U_{e1}/U_{e2})^2$  there are either 2 real solutions or 2 complex solutions and these are given by

$$\theta = -\psi_1 \pm \arctan \left[ \frac{\pm Z_1 + \sqrt{Z_2}}{Z_3} \right], \quad (9)$$

where

$$\begin{aligned} Z_1 &= U_r \cos \beta \sin \beta (k_2^2 - 1), \\ Z_2 &= (U_r - k_1^2)(1 - U_r k_2^2) - U_r \cos^2 \beta (1 - k_1^2)(1 - k_2^2), \\ Z_3 &= U_r \cos^2 \beta (k_2^2 - 1) + U_r - k_1^2, \\ \beta &= \psi_{e1} - \psi_{e2} \quad \text{and} \quad U_r = (U_{e1}/U_{e2})^2. \end{aligned}$$

The correct (real) root is taken as the solution that lies within the domain bounded by the local maxima and local minima of the curve plotted in Figure 7. This domain corresponds to  $-\pi/2 + \psi_{e1} < \theta < \pi/2 + \psi_{e2}$ , when  $\psi_{e1}$  is positive and  $\psi_{e2}$  is negative.

In practice, the complex solution may occur, this is because  $U_r$ , as calculated by the cubic calibration curves, may be slightly greater or slightly less than the local maxima or minima respectively. Occurrence of complex solutions provides a diagnostic that indicates the velocity is crossing the cone angle boundary. However, this diagnostic is not a direct measure of the number of flow vectors outside the cone angle since this number is indeterminate.

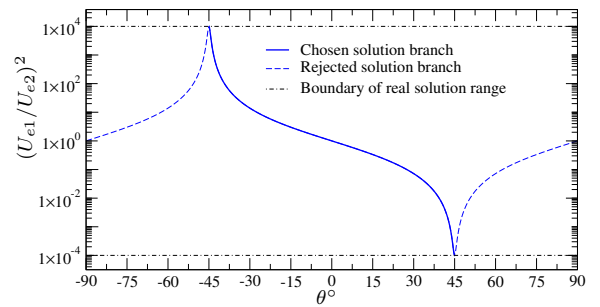


Figure 7: Velocity direction ( $\theta$ ) solution branches.

### Application of Method in a Turbulent Wake

In order to assess the calibration method further, a turbulent wake profile was measured using both a normal-wire and a cross-wire. The turbulent wake was generated by placing a circular cylinder of diameter  $D = 127$  mm in the Defence Science & Technology Low-Speed Wind Tunnel [6]. The cylinder was positioned normal to the freestream velocity, and in the horizontal plane such that it spanned the full width of the working section. End plates were fitted to isolate the tunnel wall boundary layers from the cylinder and this resulted in an effective  $L/D = 21.5$ . The freestream velocity was set to  $U_\infty = 45$  m/s

giving a Reynolds number of  $Re_D = 3.8 \times 10^5$ .

It was found that to achieve a 2-dimensional mean flow that the boundary layer had to tripped to a turbulent layer and this was achieved by placing “CADCUT” [4] gold trip dots of height 0.183 mm at 80 degrees downstream of the stagnation point.

The cross-wire probe was mounted on a traverse that provided travel in the  $y$ -direction and rotation about the  $z$  axis where the coordinate system is defined in Figure 8. The vertical roll alignment of the probe was checked by pitching probe at 40 degrees so one wire was almost normal to the free stream and imposing small roll angle changes till the output voltage was a maximum voltage.

The yaw alignment was checked using a jig which had a front silvered mirror aligned with the axis of the probe. A theodolite laser beam was aligned normal to the tunnel walls and probe adjusted so the reflected beam was coincident with the incident beam. Pitch alignment was checked with a level.

To calibrate the cross-wire, it was traversed into the freestream and pitched for a range of freestream velocities, generating the calibration data points shown in Figure 3.

The raw voltage samples were converted to instantaneous  $U$ ,  $V$  velocities in two different ways. In the first case, the full 24 point calibration was applied whereas in the second case the 7 point subset calibration was applied. The Reynolds stresses  $\overline{u^2}/U_\infty^2$ ,  $\overline{w^2}/U_\infty^2$ , and  $\overline{uv}/U_\infty^2$ , calculated using the two different calibrations, are plotted in Figure 9. The 2 calibrations give almost identical results, indicating a subset calibration is sufficient for accurate estimate of the cubic constants in (4). However, a full calibration is still required for the determination of wire angles and longitudinal cooling factors.

The normal Reynolds stresses  $\overline{u^2}/U_\infty^2$  was also measured with a normal-wire. It was found that the cross-wire and normal-wire results agreed well in the upper half of the wake profile ( $y > 0$ ) but disagreed in the lower half ( $y < 0$ ). The reason for the discrepancy in the region  $y < 0$  is not clear but may be related to higher cone angle exceedance occurring on the cross-wire in the region  $y < 0$ .

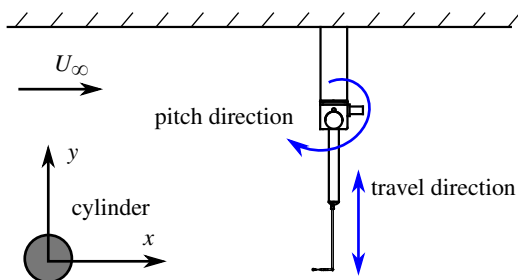


Figure 8: Experimental setup for wake traverse. The  $z$  coordinate is out of the page.

### Conclusions

A cross-wire calibration method based on an effective cooling velocity involves an initial full calibration ( $N \approx 25$  calibration points) to determine for each wire an effective wire angle and longitudinal cooling coefficient. Given these parameters, X-wire re-calibration only requires  $N \approx 7$  carefully chosen calibration points. Additionally, it has been shown that the roots to the non-linear calibration inversion can be expressed as a closed form analytic solution. There are several benefits resulting from the overall calibration method, namely the ability to

- Recalibrate X-wires very rapidly, e.g. in experiments where either anemometer drift or flow temperature vari-

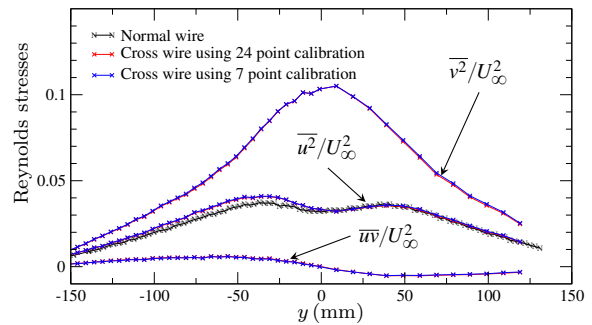


Figure 9: Wake profile measured with X-wire. Showing effect of using the  $N=24$  point compared to 7 point subset calibration. For comparison normal-wire results for  $\overline{u^2}$  are shown.

ations occur.

- Measure in-plane velocities where the flow angle variations may approach the wire angles, and therefore has applicability in highly turbulent flows.
- Identify, using the closed form analytic calibration inversion solution, those data points that have complex roots and are not valid measurements.

### References

- [1] Browne, L., Antonia, R. and Chua, L., Calibration of x-probes for turbulent flow measurements, *Experiments in Fluids*, **7**, 1988, 201–208.
- [2] Bruun, H. H., *Hot-wire anemometry*, Oxford University Press, Oxford, 1995.
- [3] Burattini, P. and Antonia, R., The effect of different x-wire calibration schemes on some turbulence statistics, *Experiments in Fluids*, **38**, 2005, 80–89.
- [4] CADCUT, <http://www.cadcut.com/services/aeronautical-testing-devices>.
- [5] Champagne, F. H., Sleicher, C. A. and Wehrmann, O. H., Turbulence measurements with inclined hot-wires Part 1. heat transfer experiments with inclined hot-wire, *J. Fluid Mech.*, **28**, 1967, 153–175.
- [6] Erm, L. P., Calibration of the flow in the extended test section of the low-speed wind tunnel at DSTO, Tech. Rep. DSTO-TR-1384, Defence Science and Technology Organisation, Melbourne, Australia, 2003.
- [7] Galassi, M., *GNU Scientific Library: Reference manual*, Network Theory Limited, Bristol, 2015.
- [8] Hinze, O., *Turbulence*, McGraw-Hill., 1959.
- [9] Jørgensen, F. E., How to measure turbulence with hot-wire anemometers - a practical guide, Technical Report 9040U6151, Dantec Dynamics, 2002.
- [10] Lomas, C. G., *Fundamentals of hot wire anemometry*, Cambridge University Press, Cambridge, 1986.
- [11] Perry, A. E., *Hot-wire Anemometry*, Clarendon Press, Oxford, 1982.
- [12] Perry, A. E., Lim, K. L. and Henbest, S. M., An experimental study of the turbulence structure in smooth- and rough-wall boundary layers, *J. Fluid Mech.*, **177**, 1987, 437–466.
- [13] Watmuff, J. H., High-speed real-time processing of cross-wire data, *Experimental Thermal and Fluid Science*, **10**, 1995, 74–85.
- [14] Webster, A. G., A note on the sensitivity to yaw of a hot-wire anemometer, *J. Fluid Mech.*, **13**, 1962, 307.
- [15] Zhao, R. and Smits, A., Binormal cooling errors in crossed hot-wire measurements, *Experiments in Fluids*, **40**, 2006, 212–217.